Food and Chemical Toxicology 129 (2019) 291–300

Contents lists available at ScienceDirect

Food and Chemical Toxicology

journal homepage: www.elsevier.com/locate/foodchemtox

Phloretin and its methylglyoxal adduct: Implications against advanced glycation end products-induced inflammation in endothelial cells

Qian Zhou[a], Jun Gong[b], Mingfu Wang[a,*]

[a] School of Biological Sciences, The University of Hong Kong, Hong Kong, China
[b] Faculty of Health Sciences, University of Macau, Macau, China

ARTICLE INFO

Keywords:
Phloretin-methylglyoxal adduct
Advanced glycation end products
Methylglyoxal
Inflammation

ABSTRACT

Methylglyoxal (MGO), a cytotoxic factor, reacts irreversibly with the side chains of lysine, cysteine, and arginine residues in proteins to form advanced glycation end products (AGEs) which might be a major pathological factor associated with diabetic complications. Thus, it is necessary to prevent or alleviate such diseases through inhibiting the formation of AGEs or lowering these AGEs-induced cellular damages. Based on our previous work, it was known that phloretin, an apple polyphenol, can inhibit the formation of AGEs under simulated physiological conditions. In this study, we found that phloretin prevented the formation of AGEs through trapping MGO in human umbilical endothelial cells (HUVECs). The phloretin-MGO adducts were analyzed in PBS and HUVECs. Surprisingly, only 1 MGO-phloretin adduct was detected in HUVECs, which was formed within 0.5 h and metabolized eventually within 24 h. The specific phloretin-MGO adduct was synthesized and identified by MS and NMR analysis. Its anti-inflammatory effect against AGEs was further investigated together with the parent compound, phloretin, which was proved to be through RAGE/p38 MAPK/NF-κB signaling pathway. Taken together, our data indicated the positive role of phloretin-MGO adduct on phloretin's protective effects, which might offer a new insight into the action mechanism of polyphenols against AGEs-induced damages.

1. Introduction

MGO is a cytosolic and highly reactive di-carbonyl compound, with a concentration ranging from 40 nM to 4.5 μM in human plasma (Kimzey et al., 2015). It can be produced *in vivo* primarily from triose phosphates in glycolysis pathway, and partly from the oxidation of aminoacetone and the degradation of glycated proteins. The intake of certain food stuffs, including sweetened soft drinks, cakes, and breads, may also contribute to intracellular MGO level. In healthy human body, 99% of MGO would be metabolized to D-lactate via the glyoxalase system (Rabbani et al., 2016). However, pathological conditions, especially diabetic complications, would lead to the abnormal accumulation of intracellular MGO. For instance, it was reported that the concentration of MGO was three times higher in the blood of diabetic patients than in healthy persons, supported by an animal study with spontaneously hypertensive rats, showing the MGO levels in plasma, aorta, kidney, and adipose tissues of hypertensive rats were significantly higher than the control (Wang et al., 2007). Unfortunately, these elevated MGO can react irreversibly with the side chains of lysine, cysteine, and arginine residues of proteins, specifically, the carbonyl group of MGO would attack these positively charged residues, and lose a molecule of H_2O, thereby leading to the formation of glycated proteins, which are generally termed as AGEs. AGEs can accumulate in a diverse range of tissues and organs, e.g., brain, heart, joint, lung, liver, and kidney, resulting in the onset or/and progression of diabetic nephropathy, hypertension, stroke, and other age-related diseases (Rabbani and Thornalley, 2014). Moreover, AGEs are recently even reported to be a critical bio-marker of cardiovascular diseases in non-diabetic patients (Nenna et al., 2015).

Phloretin (PHL), a dihydrochalcone widely distributed in the leaves and bark of apple tree and apple pericarp, was reported in the past to directly trap MGO in PBS model, and hypothesized to impede the conversion to AGEs (Shao et al., 2008). Moreover, literature data also exemplified a fact that phloretin inhibited the formation of high glucose-induced AGEs in human retinal pigment epithelial cells (Sampath et al., 2016), but the underlying inhibitory mechanism was not yet revealed. As MGO is an intermediate of AGEs, it is possible that phloretin might also directly scavenge MGO in cell model as it does in PBS medium, thus preventing the formation of AGEs. Yet, very few researches reported the detection of flavonoid-MGO conjugates in biological systems, probably due to the complexity of cellular microenvironment and relatively low reaction rate. To address this issue, in

* Corresponding author. School of Biological Sciences, The University of Hong Kong, Hong Kong, China.
E-mail address: mfwang@hku.hk (M. Wang).

https://doi.org/10.1016/j.fct.2019.05.004
Received 12 February 2019; Received in revised form 22 April 2019; Accepted 3 May 2019
Available online 04 May 2019
0278-6915/

this study, the trapping of MGO by phloretin was investigated in (HUVECs with the aid of HPLC-DAD and UPLC-Q-TOF-MS analysis.

In 2006, Lo et al. (Lo et al., 2006) provided the first line of evidence that (−)-epigallocatechin gallate (EGCG), a polyphenol from green tea could form new adducts with MGO under simulated physiological conditions. However, little is known whether these adducts have bioactivity or not. Interestingly, an anti-hyperglycemic drug metformin was reported to trap MGO and form an imidazolinone compound, which could be detected in the urine of metformin treated type-2 diabetes patients and was believed to be of therapeutic significance (Kinsky et al., 2016). More recently, Cui et al. (Cui et al., 2018) discovered that a food-grade antioxidant propyl gallate reacted with MGO in roasted pork, giving rise to a mono-MGO propyl gallate adduct which was further proved to be anti-oxidative and against carbonyl stress in lard. On this basis, it is reasonable to hypothesize that MGO-modified polyphenols might retain its parental bioactivity/properties ascribed to the remained phenolic skeleton.

Proverbially, phloretin, an apple polyphenol has a standing reputation against inflammation. As an example, phloretin was reported to decrease the expression of lipopolysaccharide (LPS)-induced pro-inflammatory cytokines through inhibiting the phosphorylation of mitogen activated protein kinases (MAPKs) in RAW 264.7 macrophages (Chang et al., 2012). Furthermore, evidences also exemplified that phloretin could attenuate inflammatory effects of thrombin via blocking the protease-activated receptor (PAR-1) induction in THP-1 monocyte/platelets/HUVECs co-cultures (Kim et al., 2014). In the present study, the protective roles of phloretin against AGEs-stimulated inflammatory responses were measured as no published data was pertinent to this specific area. In addition, to prove aforementioned hypothesis that flavonoid-MGO adducts could maintain the original bioactivity, a phloretin-MGO adduct was separated by chromatographic method, structurally elucidated by LC/MS, ^{1}H and ^{13}C NMR analysis, and its anti-inflammatory effect and action mechanism were researched together with phloretin.

2. Material and methods

2.1. Chemicals and materials

Phloretin (98%) was purchased from Natural Field Bio-technique Co., Ltd. (Xi'an, Shanxi, China). Silica gel was obtained from Jiangyou Silicone Development Co., Ltd. (Yantai, Shandong, China). Analytical grade organic reagents were from BDH Chemicals (London, UK), while HPLC grade and LC/MS grade acetonitrile (ACN) were obtained from Anaqua Chemicals Supply (Hong Kong, China). Cell counting kit-8 (CCK-8) was obtained from Dojindo Laboratories (Kumamoto, Japan). Human AGEs ELISA kit was purchased from Hebai Biological Technology Co., Ltd. (Shanghai, China). iScript advanced cDNA synthesis Kit, human interleukin 6 (IL 6) and monocyte chemoattractant protein-1 (MCP 1/CCL 2) primers, and SsoAdvanced universal SYBR green PCR kit were purchased from Bio-Rad (Hercules, CA, USA). Primary antibodies against receptor for AGEs (RAGE), p38 MAPK (t-p38), phospho-p38 MAPK (p-p38), extracellular-regulated kinase 1 and 2 (t-ERK 1/2), phospho-ERK 1/2 (p-ERK1/2), NF-κB p65 (t-p65), phospho–NF–κB p65 (p-p65), β-actin, histone H3 and anti-rabbit secondary antibodies conjugated to horseradish peroxidase (HRP) or Alexa Fluor 488 were supplied by Cell Signaling (Boston, MA, USA) and Abcam (Cambridge, MA, USA). Other reagents were from Sigma (St. Louis, MO, USA), if not specified.

2.2. Cell culture

Pooled HUVECs were obtained from Lonza Group (Basel, Switzerland). HUVECs were cultured in D-MEM/F-12 medium (Gibco Life Technologies, Carlsbad, CA, USA) supplemented with 20% fetal bovine serum (FBS), 0.1 g/L heparin sodium salt from porcine intestinal mucosa, 50 mg/L endothelial cell growth supplement (Corning, Bedford, MA, USA), 1.2 g/L sodium bicarbonate, HEPES sodium salt, and 1% Antibiotic-Antimycotic. The cells were maintained in a humidified incubator at 37 °C containing 5% CO_2, and passages 4–9 were used for all experiments.

2.3. Cell viability

HUVECs were seeded into 96-well plates at a density of 1×10^4 cells/well. After adhesion, cells were pre-incubated with different concentrations of targeted compounds for the indicated time intervals (24 or 48 h). Cell viability was detected by CCK-8 assay following the manufacturer's instructions (Hu, 2014). The results were expressed as percentage cell viability.

2.4. Evaluation of MGO-scavenging ability of phloretin in HUVECs

HUVECs were pre-incubated with 100 μM phloretin or aminoguanidine (AG) for 24 h, followed by stimulation with 50 μM MGO for 24 h. After treatment, the media were removed and the cells were scraped with 100 μL lysis buffer, and then centrifuged at 15000 rpm for 30 min. 2–4 μL supernatant was used for protein determination by the Bradford assay. 75 μL supernatant was added with 5 μL 100 μM 2, 3-butanedione (internal standard) and 5 μL 50 mM OPD to allow derivatization at 60 °C for 4 h (Miyata et al., 2000). Following that, 5 μL cold perchloric acid (70%) was added to terminate the reaction and precipitate proteins. Centrifuged at 15000 rpm for 30 min, and the supernatant was subjected to HPLC analysis. The HPLC system was a Waters 2695 module with a 2996 photodiode array detector (DAD) equipped with a reversed-phase C-18 column (4.6 mm × 250 mm, 5 μm particle size, YMC Co., Ltd. Kyoto, Japan). The mobile phase was 0.3% acetic acid and ACN, with gradient elution from 35 to 55% ACN in 21 min and a flow rate at 1 mL/min. Intracellular MGO level was determined based on the peak areas of the derivatives and normalized to the protein content of the samples (Chen et al., 2014).

2.5. Determination of the inhibitory effects of phloretin against MGO-derived AGEs formation in HUVECs

HUVECs were pretreated with 100 μM phloretin or AG for 24 h, followed by incubation with 50 μM MGO for 48 h. The media were removed and the cells were carefully scrapped on ice with 100 μL PBS. The cell suspensions were further disrupted by an ultrasonic instrument in ice bath (5 s ultrasound, 10 s interval, 20 cycles; Branson 3210, Emerson industries, Saint Louis, USA) (Yamabe et al., 2013). 50 μL supernatants were added by using a commercial AGEs kit according to the manufacturers' recommendation. The intracellular level of MGO-derived AGEs was analyzed and calculated basing on the AGEs concentration normalized to protein contents of the sample (Cha et al. 2018).

2.6. Analysis of phloretin-MGO adducts in cell-free and cell system

In cell-free system, solutions with different ratios of phloretin and MGO (6:1, 3:1, 1:1, 1:3, and 1:6) in PBS were incubated at 37 °C for 24 h. After incubation, 5 μL cold perchloric acid (70%) was added to terminate the reaction. Followed by centrifugation, the supernatants were injected into HPLC-DAD and UPLC-Q-TOF/MS for analysis. Time kinetics of phloretin and MGO (1:3) in PBS was also investigated by incubating at 37 °C for indicated time intervals. In cell system, HUVECs were seeded into 6-well plate. After adhesion, 1 mL medium with 200 μM phloretin was added into each well, and then 1 mL medium with 600 μM MGO was added into the same well (The final concentrations of phloretin and MGO were 100 and 300 μM, respectively). Mixed immediately and incubated in the cell incubator at 37 °C for indicated time intervals. After incubation, 5 μL cold perchloric acid

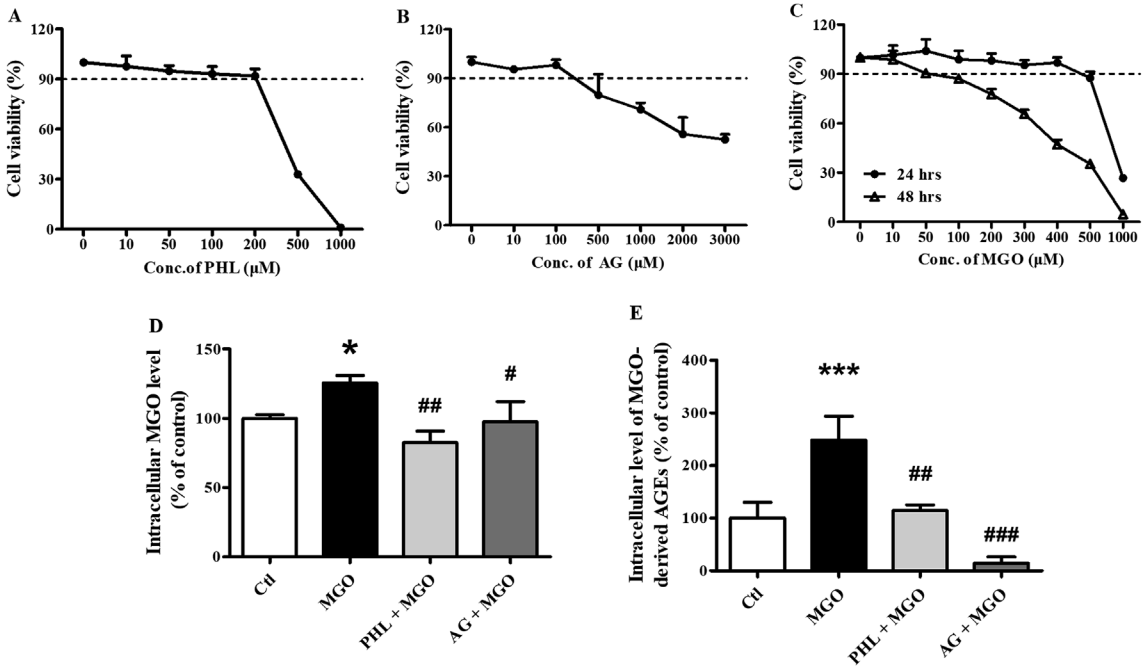

Fig. 1. Phloretin inhibits AGEs formation through trapping MGO in HUVECs. A–B: Cell viability of phloretin and AG assayed with CCK-8 kit. The incubation time was 24 h. C: Cell viability of MGO. The incubation time was 24 or 48 h. D: Intracellular MGO level by HPLC analysis. HUVECs were pretreated with 100 μM phloretin or AG for 24 h before stimulation with 50 μM MGO for 24 h. E: Intracellular AGEs level by ELISA kit. HUVECs were pretreated with 100 μM phloretin or AG for 24 h before stimulation with 50 μM MGO for 48 h $*p < 0.05$ vs. control, $***p < 0.001$ vs. control. $\#p < 0.05$ vs. AGEs-treatment, $\#\#p < 0.01$ vs. AGEs-treatment, $\#\#\#p < 0.001$ vs. AGEs-treatment.

(70%) was added to terminate the reaction and precipitate proteins. All these solutions were centrifuged at 15000 rpm for 30 min before the injection into HPLC-DAD or LC/MS for analysis.

For HPLC-DAD analysis, a RP C-18 column (250 × 4.6 mm, 5 μm, YMC Co., Ltd. Kyoto, Japan) was used. The mobile phase was 0.1% formic acid in water (v/v) and ACN, with gradient elution from 35 to 60% ACN in 31 min and a flow rate of 1 mL/min. For UPLC-Q-TOF/MS analysis, MS was operated on a Sciex X500 Quadrupole Time-of-Flight (Q-TOF) system, using ionspray set at 4500 V, curtain gas at 35, drying temperature at 350 °C, collision energy (CE) at 10 V (negative mode), and mass spectra were scanned from *m/z* 100 to 1000. The targeting spectrum were extracted (Infante et al., 2006). The column was a YMC RP C-18 column (150 × 2.0 mm, 5 μm, YMC Co., Ltd. Kyoto, Japan). The mobile phase was composed of water with 0.1% formic acid and ACN, isocratically eluted with 30% ACN and a flow rate of 0.4 mL/min.

2.7. Separation and identification of di-MGO phloretin (DMP) adduct

220 mg phloretin and 0.68 mL MGO (40% solution, Sigma) were added into 1 L PBS and incubated at 37 °C for 2 h in the dark. Then the solution was extracted by 1 L ethyl acetate and evaporated under 35 °C by a rotary vacuum evaporator. The residue was re-dissolved in ethyl acetate and loaded onto a silica gel column (100–200 mesh) eluted with 1: 1 ecthyl acetae and n-hexsane mixtures to obtain DMP (150 mg, 98%). The purified product was analyzed by LC/UV, LC/MS, and NMR (^{1}H, ^{13}C) analysis. The LC/UV and LC/MS procedures were listed in 2.6. All NMR analysis were acquired on a 400 MHz Bruker instrument (Billerica, MA, USA) at 25 °C, with compound dissolved in CD_3OD in a 3 mm i.d. tube. The chemical shift assignments were referenced internally to TMS at 0 ppm (Shao et al., 2008). The purified product was named as DMP-A and stored at −80 °C until use.

2.8. Preparation of MGO-derived AGEs

MGO-derived AGEs, also named as AGE-4, were prepared according to the protocol of Meeprom et al. (Meeprom et al., 2015) with slight modification. 10 mg/mL BSA was incubated with/without 55 mM MGO in PBS for 8 days at 37 °C. After incubation, both AGEs (MGO-BSA) and control BSA were dialyzed against PBS for 2 days at 4 °C. The glycation level was detected by a fluorescence spectrophotometer (excitation at 370 nm and emission at 440 nm), and the protein concentration was measured by the Bradford protein assay using BSA as standard (Lee and Lee, 2007). The relative fluorescence intensity of the AGEs to control BSA was ~50-fold. The AGEs were stored at −20 °C until use.

2.9. Quantitative real-time PCR (qPCR)analysis of MCP 1 and IL 6

HUVECs were pre-incubated with 10 μM of DMP-A or phloretin for 24 h, followed by stimulation with AGEs (500 μg/mL, 48 h). After treatments, total RNAs were extracted with standard TRIzol (Life Technologies, Foster City, CA, USA) method and the concentrations of RNAs were detected by a spectrophotometer equipped with a μDrop™ plate (Multiskan TM GO, Thermo Fisher Scientific Inc., USA). Then 1 μg total RNAs was reverse transcribed using a iScript advanced cDNA synthesis Kit. mRNA levels of MCP 1, IL 6, and glyceraldehyde-3-phosphate dehydrogenase (GAPDH) were measured by qPCR using the SsoAdvanced universal SYBR green supermix. The values were normalized by GAPDH expression and data were analyzed using the ΔΔCT method (Yu et al., 2018).

2.10. Western blot analysis

HUVECs were seeded into 6-well plate, pre-incubated with 10 μM DMP-A or phloretin for 24 h, and stimulated with 500 μg/mL AGEs for 0.5 h (for phosphorylated proteins) or 48 h. After treatment, the proteins were extracted with RIPA lysis buffer (Sigma-Aldrich, St. Louis, USA) containing a protease inhibitor with/without a phosphotase inhibitor cocktail (Sigma-Aldrich, St. Louis, USA). The protein contents were quantified with the Bradford dye-binding assay. 5–10 μg protein lysates were resolved on 10% SDS-polyacrylamide gel and

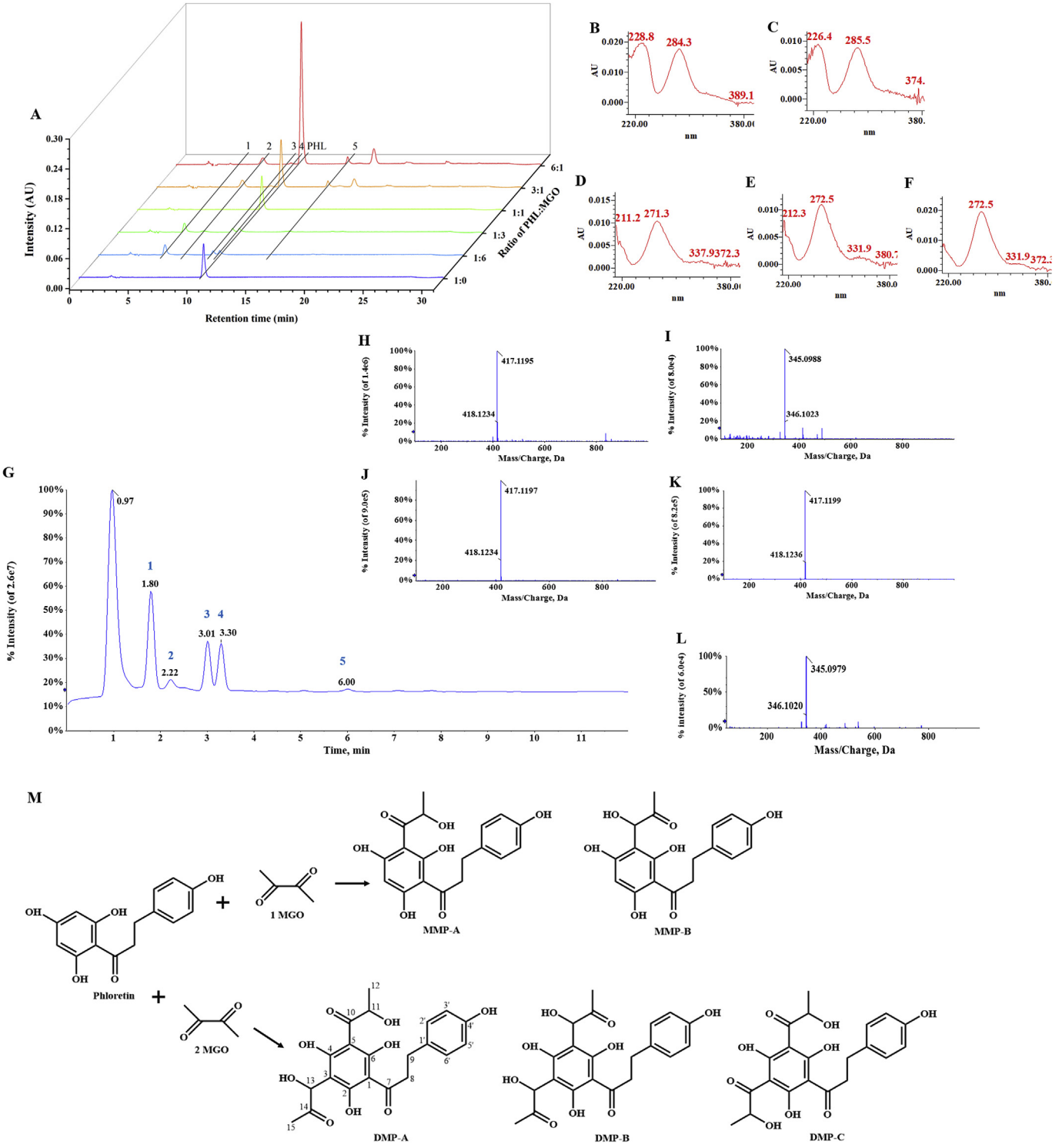

Fig. 2. Characterization of phloretin and MGO reactions in cell-free system. A: HPLC chromatography of different ratio of phloretin and MGO (6:1–1:6) in PBS. B–D: UV absorption spectrum of compound 1–5. F: TIC of phloretin and MGO (1:3) in PBS. G–J: XICs of compound 1–5. G: Proposed formation pathway of phloretin and MGO adducts.

electrophoretically transferred to polyvinylidene difluoride membranes (Bio-Rad, Hercules, CA, USA). After blocking in 3–5% BSA or milk in TBST (Tris-buffered saline containing 0.1% Tween 20) for 1 h at room temperature, the membranes were incubated with the specific primary antibodies overnight at 4 °C, washed with TBST, incubated with the appropriate secondary antibodies for 1 h at room temperature, and visualized with a Chemiluminescence detection kit (ECL, Thermo Fisher Scientific). Quantification was performed using Image J software (National Institute of Health, Bethesda, MD, USA). β-Actin served as a loading control (Li et al., 2017).

2.11. Preparation of nuclear and cytosolic fractions of NF-κB

HUVECs were seeded into 6-well plate, pre-incubated with 10 μM DMP-A or phloretin for 24 h, and stimulated with 500 μg/mL AGEs for 0.5 h. After treatment, nuclear and cytosolic proteins were extracted

Table 1
Chromatographic, UV–Vis, and Mass Spectroscopy Characteristics of phloretin-MGO adducts.

No.	Compound	t_R (min)	UV λ_{max} (nm)	MW	$[M-H]^-$
1	Di-MGO-phloretin	5.6	228, 284	418	417.1195
2	Mono-MGO-phloretin	7.3	226, 285	346	345.0988
3	Di-MGO-phloretin	9.7	271	418	417.1197
4	Di-MGO-phloretin	10.3	272	418	417.1199
5	Mono-MGO-phloretin	14.5	272	346	345.0979
	Phloretin	10.6	224, 285	274	273.1056

with a Nuclear and Cytoplasmic Extraction Reagents kit (Pierce Biotechnology, Rockford, IL, USA) according to the manufacturer's instruction. All steps were carried out on ice or at 4 °C unless stated otherwise (Song et al., 2012). The nuclear and cytosolic fractions obtained were incubated with primary antibody against t-p65.

2.12. Immunohistochemical analysis of NF-κB

HUVECs were grown on 0.01% poly-L-lysine coated glass slides in 24-well plates. After adhesion, cells were pre-treated with 10 μM DMP-A or phloretin for 24 h, followed by incubation with 500 μg/mL AGEs for 0.5 h. Then the cells were fixed with 4% paraformaldehyde for 20 min at room temperature, and permeabilized with 0.1% Triton X-100 in PBS solution for 10 min at 4 °C. Following that, the slides were washed with PBS, blocked in 4% BSA in PBS solution for 30 min at room temperature, and incubated with t-p65 primary antibody overnight at 4 °C. The cells were then washed with PBS, incubated with secondary antibody in the dark for 1 h at room temperature, washed with PBS again, and stained with 0.3 μM DAPI for 5 min. Finally, the slides were observed under a fluorescence microscope (80i, Nikon instruments Inc., USA) (Verma and Manna, 2016).

2.13. Statistical analysis

All experiments were repeated at least three times. The data were analyzed using one-way analysis of variance (ANOVA) followed by a Turkey's test for comparing the group means. Graph Pad Prizm version 6.0 for Windows (GraphPad Software, Inc.) were used to draw graphs and to perform statistical analyses. p values of < 0.05 were considered as statistically significant.

3. Results and discussion

3.1. Phloretin inhibits the formation of MGO-derived AGEs through trapping MGO in HUVECs

The direct trapping of MGO is known as one of the major mechanisms to prevent the formation of AGEs (Sompong and Adisakwattana, 2015). On account of published data, AG was used as positive control for its noted MGO-trapping ability both *in vitro* and *in vivo* (Crascì et al., 2018). In the first instance, the cell viabilities of phloretin, AG, and MGO were measured by CCK-8 assay to figure out a

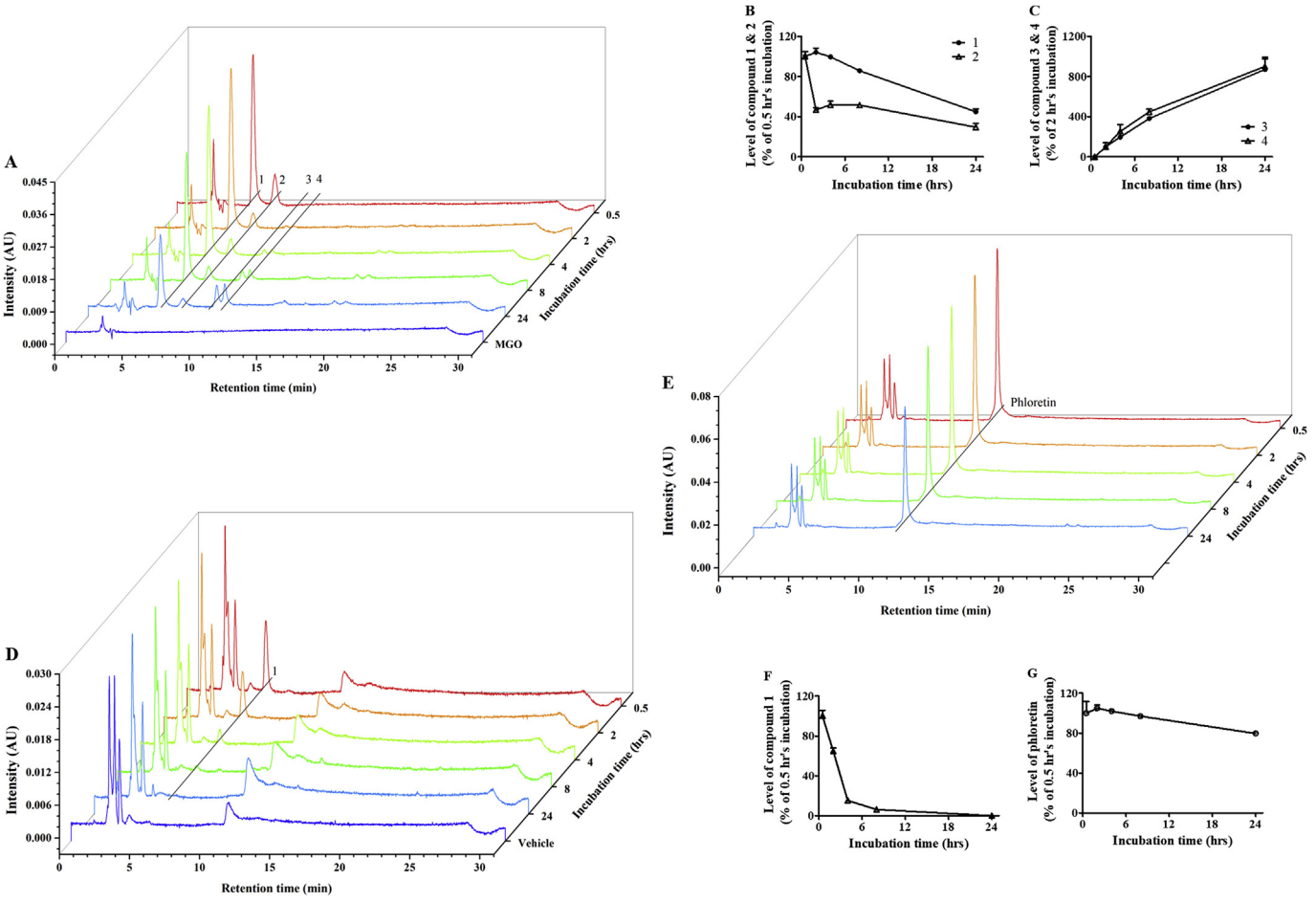

Fig. 3. Time kinetics of phloretin and MGO reactions in cell-free and cell systems. A: HPLC chromatography of phloretin and MGO (1:3) during 24 h incubation in PBS. B–C: Level change of newly formed adducts during 24 h incubation in PBS. D: HPLC chromatography of phloretin and MGO (1:3) in the medium of HUVECs during 24 h incubation. E: HPLC chromatography of phloretin (100 μM) in the medium of HUVECs during 24 h incubation. F: Level change of compound 1 in the medium of HUVECs during 24 h incubation. G: Level change of phloretin in the medium of HUVECs during 24 h incubation.

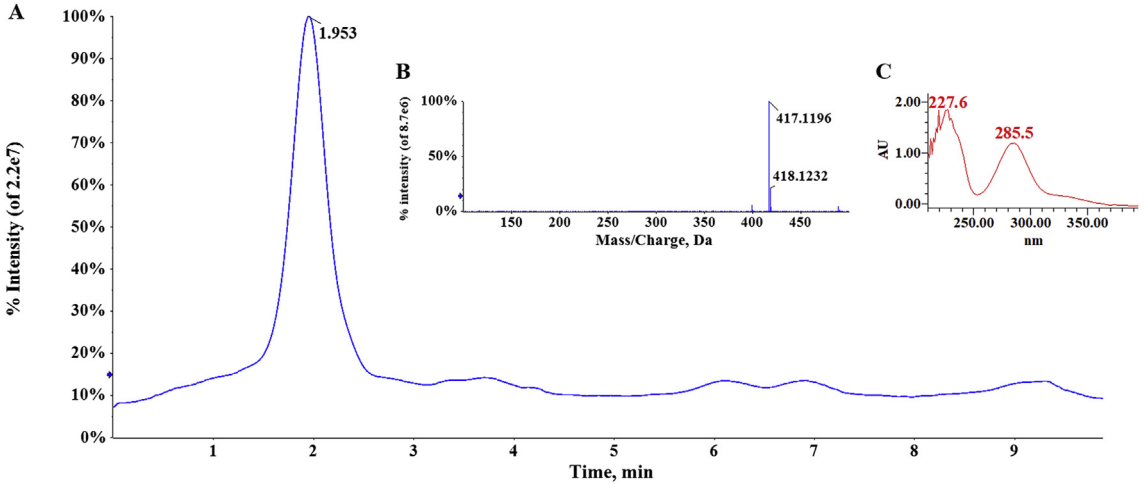

Fig. 4. Chromatography of DMP-A. A: TIC. B: XIC. C: UV absorption spectrum.

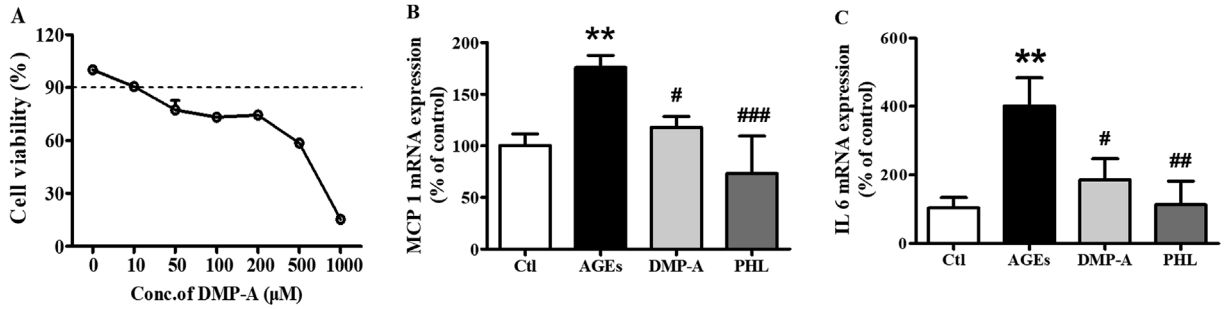

Fig. 5. Phloretin and its MGO adduct decrease AGEs-induced inflammation in HUVECs. A: Cell viability of DMP-A. The incubation time was 24 h. B: MCP 1 gene expression by qPCR assay. C: IL 6 gene expression by qPCR assay. HUVECs were pretreated with 10 μM DMP-A or phloretin for 24 h before stimulation with 500 μg/mL AGEs for 48 h. $^{**}p < 0.01$ vs. control. $\#p < 0.05$ vs. AGEs-treatment, $\#\#p < 0.01$ vs. AGEs-treatment, $\#\#\#p < 0.001$ vs. AGEs-treatment.

proper dosage in HUVECs. As shown in Fig. 1A–B, the cell viabilities decreased correspondingly when incubated with increased level of phloretin (0–1000 μM) or AG (0–3000 μM) for 24 h. Upon careful consideration, the concentration 100 μM was used for phloretin and AG in the following experiments. As for MGO, the incubation time was 24 h or 48 h, and 50 μM was adopted (Fig. 1C). Following that, the intracellular levels of MGO and MGO-derived AGEs were measured. It was found that pre-incubation of HUVECs with phloretin (100 μM, 24 h) before treatment with MGO (50 μM, 24 h) remarkably decreased the intracellular MGO content, which was even lower than AG pre-treatment (100 μM, 24 h; Fig. 1D). Intracellular AGEs level was detected via an ELISA kit. HUVECs were pre-treated with 100 μM phloretin or AG for 24 h, followed by incubation with 50 μM MGO for 48 h. MGO treatment alone led to an increase in AGEs level by approximately 1.5 times, whereas phloretin pre-incubation reversed the situation and decreased AGEs to normal level (Fig. 1E). Therefore, it can be concluded that phloretin significantly prevented the formation of MGO-derived AGEs through direct trapping of over-dosed intracellular MGO in HUVECs.

3.2. Reaction kinetics of phloretin-MGO adducts in cell-free and cell system

Plant-derived polyphenols, including quercetin, naringenin, and procyanidin B_2, have been demonstrated to be antiglycative in cell-free models (Sadowska-Bartosz et al., 2014). In general, prolonged incubation times, e.g., 24 or 48 h, were adopted, which may apparently cover the discrepancies of inhibitory rate and the dynamic compositions of newly formed adducts. In this study, kinetic analysis of phloretin and MGO was done both in cell-free (PBS) and cell (HUVECs) system. Fig. 2A showed the HPLC chromatography of phloretin and MGO incubated in PBS for 24 h at diverse ratios (phloretin: MGO = 6:1, 3:1, 1:1, 1:3, or 1:6). 100 μM phloretin (phloretin: MGO = 1:0) was used as a reference. Basically, five new adducts were detected and temporarily named as compound 1–5. Fig. 2B–F showed the maximum UV absorbance (UV λ_{max}) of these compounds. To gain more compound information, the reaction mixture of ratio 1:3 was injected into LC/MS using the negative mode. The total ion chromatogram (TIC) and extracted ion chromatograms (XICs) were shown in Fig. 2G-L via 30% ACN elution. Compound 1, 3, and 4 exhibited an identical deprotonated molecular ion peak $[M-H]^-$ at m/z 411.119 ($C_{21}H_{22}O_9$), corresponding to the adducts formed by two molecules of MGO with phloretin, while compound 2 and 5 generated $[M-H]^-$ at m/z 345.098 ($C_{18}H_{18}O_7$), which corresponded to the adduct formed by a molecule of MGO with phloretin. With reference to the literature data (Shao et al., 2008; Shao et al., 2014), compound 1, 3, and 4 are di-MGO conjugated phloretin, while compound 2 and 5 are mono-MGO conjugated phloretin. Their retention time (t_R), UV λ_{max}, MW, and $[M-H]^-$ were summarized in Table 1. Fig. 2M showed the proposed formation pathway for mono-MGO and di-MGO phloretin adducts, with MGO reacted with the C3 or/and C5 position at the A ring through two different conjugating ways.

Time kinetics of new adducts in cell-free and cell system during 0.5–24 h incubation were shown in Fig. 3 (the ratio of phloretin: MGO = 1:3). In the cell-free system, only compound 1 and 2 were formed at the beginning (Fig. 3A). The level of compound 1 peaked at the second hour, and then decreased to ~50% at 24 h incubation compared with the 0.5 h's data, whereas compound 2 decreased all through the time (Fig. 3B). To the opposite, the compound 3 and 4 increased gradually from the start to the end (Fig. 3C). To sum up, compound 1 (a di-MGO phloretin) is the predominant product of phloretin and MGO (ratio at 1:3) in PBS model. The formation rate of compound 1 is fast, although it would convert to other adducts during

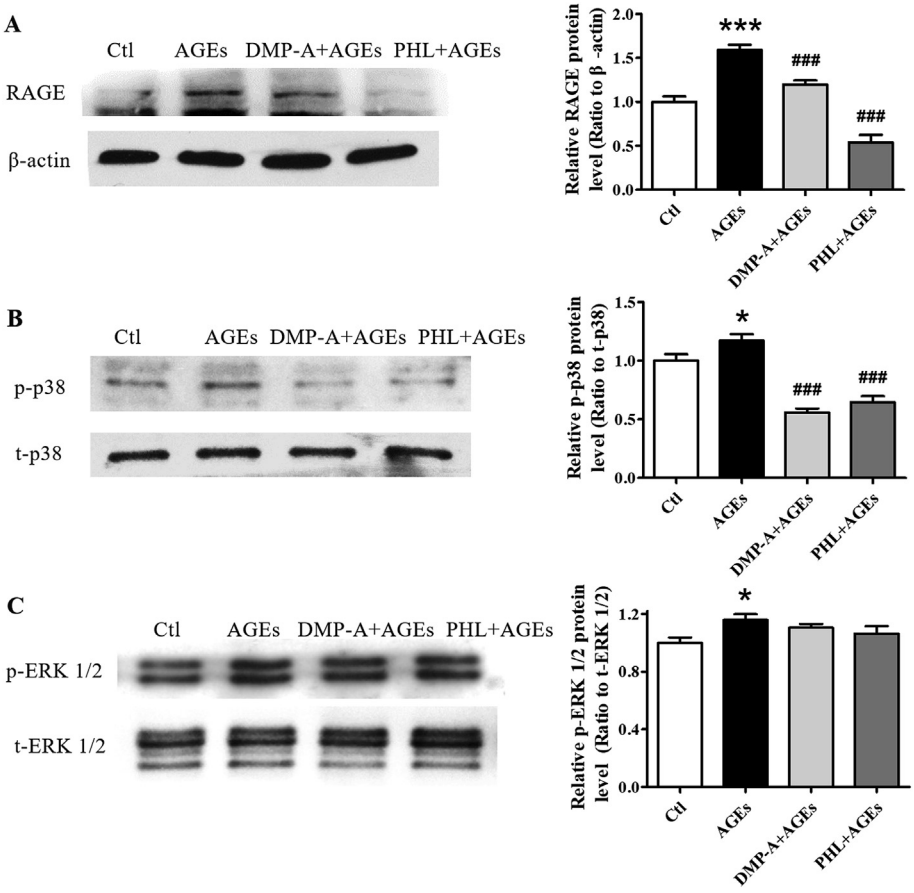

Fig. 6. The anti-inflammatory abilities of phloretin and its MGO adduct through RAGE/p38 MAPK. A: Protein expression of RAGE by Western blot. HUVECs were pre-treated with 10 μM DMP-A or phloretin for 24 h before stimulation with 500 μg/mL AGEs for 48 h. β-Actin served as a control. B–C: Protein expression of p/t-p38 and p/t-ERK 1/2. HUVECs were pre-treated with 10 μM DMP-A or phloretin for 24 h before stimulation with 500 μg/mL AGEs for 30 min. Total cell lysates were obtained by lysis in RIPA containing protease with/without phosphatase inhibitor cocktail. Fold changes were quantified with Image J software. $^{*}p < 0.05$ vs. control, $^{***}p < 0.001$ vs. control. $###p < 0.001$ vs. AGEs-treated HUVECs.

long-time reaction. In HUVECs, only compound 1 was found in the medium (Fig. 3D), whose level was decreasing from the first time point to almost below detection line after 8 h's incubation (Fig. 3F) and its peak area was ~30% of PBS model at the same half an hour incubation. The new adducts in the cell lysis of HUVECs were also investigated, but none was detected. Fig. 3E and G showed the dynamic level of 100 μM phloretin during 24 h incubation in the media of HUVECs. Phloretin remained an almost unchanged high level during the first 8 h, following by a slight decreasing to ~80% at 24 h, indicating that the utilization of pure phloretin in HUVECs was relatively slow. In the light of Fig. 3, it seems that phloretin trapped MGO to form compound 1 at a fast reaction rate in biological system, which effectively ameliorated the dicarbonyl stress and prevented its further damage to proteins. However, the formed compound 1 in the cell model were metabolized soon to under the detection line of UV detector.

3.3. Separation and identification of the phloretin and MGO adduct

Compound 1 was purified from the reaction of phloretin and MGO at a 1:6 ratio using a silica gel column eluted with hexane and ethyl acetate (1:1) mixture. Its t_R of LC/MS (1.9 min), $[M-H]^-$ (417.1197), and UV λ_{max} (227 and 285 nm) were shown in Fig. 4, and its structure was established by analyzing the ^1H, ^{13}C, DEPT-90, and DEPT-135 NMR spectra. ^1H NMR (400 MHz, CD_3OD, 25 °C, TMS): δ = 7.09 (d, J = 7.6 Hz, 2H; H-2″ and H-6″), 6.71 (d, J = 7.7 Hz, 2H; H-3″ and H-5″), 4.62 (s, 1H; H-13′), 4.11 (dd, J = 14.0, 6.9 Hz, 1H; H-11′), 3.27 (d, J = 6.4 Hz, 2H; H-8′), 2.89 (s, 2H; H-9′), 2.08 (d, J = 39.2 Hz, 3H; H-12′), 1.69 ppm (s, 3H; H-15′). The ^1H NMR spectrum showed a distinct AA'BB' set for four protons at δ = 7.09 (J = 7.6 Hz) and 6.71 ppm (J = 7.7 Hz), indicating a para-substituted benzene ring, which was similar to those of phloretin (HMDB0003306, Human Metabolome Database). Phloretin has a distinct 1H signal at δ = 5.81 ppm (s), while our compound had no signal around 5.81 ppm indicating both the C3 and C5 positions of the A ring were conjugated with MGO. However, two different sets of proton signals for MGO were detected: δH 4.11 (1H), 2.08 (3H) and 4.62 (1H), 1.69 (3H), leading to the consideration of different MGO conjugated pathway. ^{13}C NMR (400 MHz, CD_3OD, 25 °C, TMS): δ = 209.41 (s, C-7), 204.84 (s, C-14), 172.39 (s, C-10), 165.27 (s, C-1), 164.99 (s/d C-3), 163.14 (s, C-5), 155.96 (s, C-4′), 132.88 (s, C-1′), 129.77 (s; C-2′ and C-6′), 115.51 (s, C-3′ and C-5′), 107.46 (s, C-2), 105.28 (s, C-4), 101.86 (s, C-6), 75.27 (s d, C-13), 71.73 (s d, C-11), 45.50 (s, C-8), 30.47 (s, C-9), 24.81 (s, C-15), 24.27 (s, C-12). In general, ^1H and ^{13}C results confirmed the structure of compound 1 as DMP-A, with its nomenclature as 2-hydroxy-1-(2,4,6-trihydroxy-3-(1-hydroxy-2-oxopropyl)-5- (3-(4-hydroxyphenyl)propanoyl)phenyl) propan-1-one. To the best of our knowledge, this is the first time to identify a di-MGO phloretin adduct.

3.4. Phloretin and its MGO adduct ameliorate AGEs-induced inflammation in HUVECs

The interaction of AGEs with endothelial cells, as well as other cell types, eventually activates the propagation process of inflammation, which provides a mechanism to augment vascular dysfunction and diabetic vasculopathy (Basta et al., 2004). MCP 1, a pro-inflammatory cytokine, can activate macrophages and recruit monocytes to the sites of injuries, which accelerates the inflammatory responses (Chao et al., 2010). IL 6 is a multifunctional cytokine with a wide range of biological activities, including as a central mediator of inflammation (Chen et al., 2013). Therefore, it is possible to attenuate AGEs-induced inflammation through decreasing the expression of these cytokines. To investigate the protective effects of phloretin and its MGO adduct on AGEs-induced inflammation, qPCR was performed to evaluate changes in the transcription levels of MCP 1 and IL 6 in HUVECs in response to the

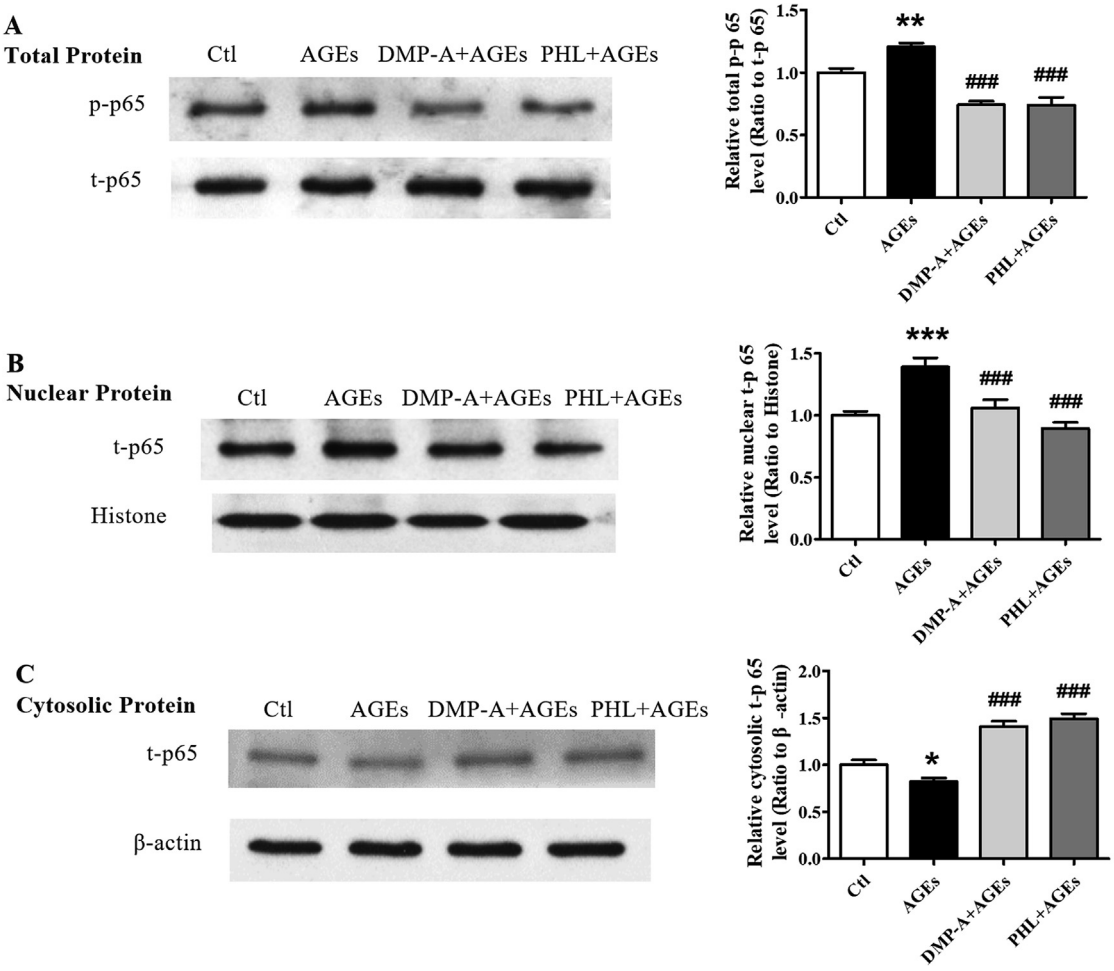

(caption on next page)

treatment with phloretin and it MGO-adduct, DMP-A, respectively. The cell viability of DMP-A was assayed in the first place (Fig. 5A), which showed a relatively higher cytotoxicity than phloretin (Fig. 1A). To better compare the anti-inflammatory ability of the two compounds, the same concentration of 10 μM was adopted for the following experiments. In accordance with expectations, AGEs (500 μg/mL, 48 h)

Fig. 7. Phloretin and its MGO adduct inhibit AGEs-induced phosphorylation and trans-localization of NF-κB. HUVECs were pre-treated with 10 μM DMP-A or phloretin for 24 h before stimulation with 500 μg/mL AGEs for 30 min. A–C: Total, cytosolic, and nuclear protein expression of NF-κB by Western blot. Total cell lysates were obtained by lysis in RIPA buffer containing protease and phosphatase inhibitor cocktail. Cytoplasmic and nuclear proteins were extracted and resolved, β-actin (total protein and cytosolic fraction) and histone H3 (nuclear fraction) served as loading controls. Fold changes were quantified with Image J software. D: Trans-localization of NF-κB by immunocytochemistry analysis. After treatment, cells were fixed, permeabilized, bound with t-p65 antibody overnight and then with secondary antibody conjugated with Alexa Fluor® 488 (Green). Cell nuclei were stained with 0.3 μM DAPI (Blue) for 5 mins and visualized by fluorescence microscopy. The merged pictures represented the combined image of NF-κB fluorescence and nuclear staining. $*p < 0.05$ vs. control, $**p < 0.01$ vs. control, $***p < 0.001$ vs. control. $\#\#p < 0.01$ vs. AGEs-treated HUVECs, $\#\#\#p < 0.001$ vs. AGEs-treated HUVECs. (For interpretation of the references to colour in this figure legend, the reader is referred to the Web version of this article.)

significantly ($p < 0.01$, $p < 0.01$) increased the mRNA levels of MCP 1 and IL 6 in HUVECs, whereas the pretreatment of cells with 10 μM DMP-A or phloretin for 24 h remarkably down-regulated the levels of these cytokines. Phloretin pre-treatment effectively lowered the increased expression of these cytokines by 103% ($p < 0.001$; Fig. 5B) and 289% ($p < 0.01$; Fig. 5C). DMP-A pre-incubation also alleviated AGEs-induced overexpression of MCP 1 and IL 6 by 58% ($p < 0.05$; Fig. 5B) and 216% ($p < 0.05$; Fig. 5C), respectively. Besides, the anti-inflammatory effects of DMP-A and phloretin showed no significant difference, although phloretin seemed to have a higher inhibition rate.

3.5. Anti-inflammation via RAGE/p38 MAPK/NF-κB pathway

RAGE is a major receptor for AGEs, which widely distributes on the cell surface of monocytes, macrophages, neurons, endothelial cells, and smooth muscle cell (Tanikawa et al., 2009). It is reported that AGEs-RAGE interaction initiates the phosphorylation of MAPKs, including ERK 1/2 and p38, which subsequently lead to the aberrant activation of NF-κB, while NF-κB acts as a master regulator of inflammation, mediating the genes expressions of both innate and adaptive immune responses. Furthermore, the activation of NF-κB in return induces the expression of RAGE, resulting in a closed loop that upregulates inflammatory responses (Basta et al., 2004; Davis et al., 2016). Therefore, decreasing the level of RAGE can be an essential pathway to prevent AGEs-induced inflammation. Our data showed that RAGE protein expression was elevated to 1.6-fold by AGEs treatment (500 μg/mL, 48 h), whereas DMP-A and phloretin pre-treatment (10 μM, 24 h) significantly reversed the situation, revealing the positive role of phloretin and its MGO adduct against AGEs-stimulated cellular damages (Fig. 6A). To better understand the action mechanism, the activation of ERK 1/2, p38, and NF-κB were measured by Western blot. The phosphorylation of these proteins was reported to follow a time dependent manner, and AGEs significantly induced the phosphorylated proteins expression at 20–120 min incubation (Zhang et al., 2016). Our data verified that the relative level of phosphorylated ERK 1/2 and p38 to their total proteins were significantly induced by AGEs-treatment (500 μg/mL, 30 min) (Fig. 6B–C). DMP-A and phloretin pre-treatment (10 μM, 24 h) dramatically prevented the action of p38, although both compounds seemed to be out of effect on ERK 1/2. NF-κB is normally regulated by its inhibitory protein IκBα, which sequestrates NF-κB and keeps it in the cytoplasm. Stimulus signals, including LPS and AGEs, lead to the phosphorylation of IκBα, thus liberating NF-κB and enabling it into the nucleus, where it binds to specific response elements in DNA and activates the expression of inflammatory cytokines (Pradère et al., 2016). As shown in Fig. 7A, AGEs treatment (500 μg/mL, 30 min) significantly induced the phosphorylation of p65 in the whole cell lysates of HUVECs, whereas DMP-A and phloretin pre-incubation (10 μM, 24 h) dramatically decreased the ratio level of p-p65 to t-p65. The trans-localization of t-p65 was measured by both immunoblotting of the cytosolic and nuclear fractions and immunocytochemical analysis. As shown in Fig. 7B–C, DMP-A and phloretin pretreatment effectively inhibited AGEs-induced translocation of t-p65. Consistently, the immunofluorescence images (Fig. 7D) provided strong evidence that the two compounds substantially prevented the action. Therefore, our data indicated that the protective effect of phloretin was likely through RAGE/p38 MAPK/NF-κB pathway. Moreover, it is the first time to report the bioactivity of a chalcone-MGO adduct, which showed a similar anti-inflammatory property with its parental compound, indicating a positive role of flavonoid-MGO adducts.

4. Conclusions

In summary, the present study demonstrates that phloretin, an apple polyphenol, effectively inhibits the formation of AGEs through scavenging MGO in HUVECs. In the process, phloretin reacts with MGO to form a di-MGO phloretin conjugate in the medium of HUVECs. The specific adduct is separated for the first time and further identified as 2-hydroxy-1-(2,4,6-trihydroxy-3-(1-hydroxy-2-oxopropyl)-5-(3-(4-hydroxyphenyl)propanoyl)phenyl)propan-1-one by LC/MS and NMR analysis. Moreover, this study provides strong evidence that the newly formed adduct, as well as its parent compound is significant in preventing AGEs-induced inflammation though RAGE/p38 MAPK/NF-κB pathway. The findings suggest the dual effects of phloretin via preventing the formation of AGEs and its di-MGO conjugate against AGEs-induced inflammation, which mediately proves the proverb “an apple a day keeps the doctor away”.

Disclosure of potential conflicts of interest

The authors declare that there are no conflicts of interest.

Source of funding

This study was supported by Hong Kong General Research Fund (17111715).

Acknowledgement

We are grateful for the excellent technical assistance of Ms. Dorothy M.C. Chan.

Transparency document

Transparency document related to this article can be found online at https://doi.org/10.1016/j.fct.2019.05.004

References

Basta, G., Schmidt, A.M., De Caterina, R., 2004. Advanced glycation end products and vascular inflammation: implications for accelerated atherosclerosis in diabetes. Cardiovasc. Res. 63 (4), 582–592.

Cha, S.H., Hwang, Y., Heo, S.J., Jun, H.S., 2018. Diphlorethohydroxycarmalol attenuates methylglyoxal-induced oxidative stress and advanced glycation end product formation in human kidney cells. Oxidative Med. Cell. Longev. 1–14 2018.

Chang, W.T., Huang, W.C., Liou, C.J., 2012. Evaluation of the anti-inflammatory effects of phloretin and phlorizin in lipopolysaccharide-stimulated mouse macrophages. Food Chem. 134 (2), 972–979.

Chao, C.Y., Mong, M.C., Chan, K.C., Yin, M.C., 2010. Anti-glycative and anti-inflammatory effects of caffeic acid and ellagic acid in kidney of diabetic mice. Mol. Nutr. Food Res. 54 (3), 388–395.

Chen, X.Y., Huang, I.M., Hwang, L.S., Ho, C.T., Li, S., Lo, C.Y., 2014. Anthocyanins in blackcurrant effectively prevent the formation of advanced glycation end products by trapping methylglyoxal. J. Funct. Foods 8, 259–268.

Chen, Y.J., Sheu, M.L., Tsai, K.S., Yang, R.S., Liu, S.H., 2013. Advanced glycation end products induce peroxisome proliferator-activated receptor γ down-regulation-related inflammatory signals in human chondrocytes via Toll-like receptor-4 and

receptor for advanced glycation end products. PLoS One 8 (6), 1–10.
Crascì, L., Lauro, M.R., Puglisi, G., Panico, A., 2018. Natural antioxidant polyphenols on inflammation management: anti-glycation activity vs metalloproteinases inhibition. Crit. Rev. Food Sci. Nutr. 58 (6), 893–904.
Cui, H., Tao, F., Hou, Y., Lu, Y., Zheng, T., Sang, S., Lv, L., 2018. Dual effects of propyl gallate and its methylglyoxal adduct on carbonyl stress and oxidative stress. Food Chem. 265, 227–232.
Davis, K.E., Prasad, C., Vijayagopal, P., Juma, S., Imrhan, V., 2016. Advanced glycation end products, inflammation, and chronic metabolic diseases: links in a chain? Crit. Rev. Food Sci. Nutr. 56 (6), 989–998.
Hu, S., 2014. Resorcinol-type Phenolic Compounds from Natural Sources Inhibit α-MSH Induced Melanogenesis and UVA-Induced DNA Damage. HKU Theses Online (HKUTO).
Infante, H.G., O'Connor, G., Rayman, M., Hearn, R., Cook, K., 2006. Simultaneous identification of selenium-containing glutathione species in selenised yeast by on-line HPLC with ICP-MS and electrospray ionisation quadrupole time of flight (QTOF)-MS/MS. J. Anal. Atomic Spectrom. 21 (11), 1256–1263.
Kim, M.S., Park, S.H., Han, S.Y., Kim, Y.H., Lee, E.J., Yoon Park, J.H., Kang, Y.H., 2014. Phloretin suppresses thrombin-mediated leukocyte-platelet-endothelial interactions. Mol. Nutr. Food Res. 58 (4), 698–708.
Kimzey, M.J., Kinsky, O.R., Yassine, H.N., Tsaprailis, G., Stump, C.S., Monks, T.J., Lau, S.S., 2015. Site specific modification of the human plasma proteome by methylglyoxal. Toxicol. Appl. Pharmacol. 289 (2), 155–162.
Kinsky, O.R., Hargraves, T.L., Anumol, T., Jacobsen, N.E., Dai, J., Snyder, S.A., Monks, T.J., Lau, S.S., 2016. Metformin scavenges methylglyoxal to form a novel imidazolinone metabolite in humans. Chem. Res. Toxicol. 29 (2), 227–234.
Lee, S.J., Lee, K.W., 2007. Protective effect of (-)-epigallocatechin gallate against advanced glycation endproducts-induced injury in neuronal cells. Biol. Pharm. Bull. 30 (8), 1369–1373.
Li, F., Lang, F., Zhang, H., Xu, L., Wang, Y., Zhai, C., Hao, E., 2017. Apigenin alleviates endotoxin-induced myocardial toxicity by modulating inflammation, oxidative stress, and autophagy. Oxidative Med. Cell. Longev. 1–10 2017.
Lo, C.Y., Li, S.M., Tan, D., Pan, M.H., Sang, S.M., Ho, C.T., 2006. Trapping reactions of reactive carbonyl species with tea polyphenols in simulated physiological conditions. Mol. Nutr. Food Res. 50 (12), 1118–1128.
Meeprom, A., Sompong, W., Suantawee, T., Thilavech, T., Chan, C.B., Adisakwattana, S., 2015. Isoferulic acid prevents methylglyoxal-induced protein glycation and DNA damage by free radical scavenging activity. BMC Complement Altern. Med. 15 (1), 346.
Miyata, T., Ueda, Y., Asahi, K., Izuhara, Y., Inagi, R., Saito, A., De Strihou, C.V.Y., Kurokawa, K., 2000. Mechanism of the inhibitory effect of OPB-9195 [(±)-2-isopropylidenehydrazono-4-oxo-thiazolidin-5-ylacetanilide] on advanced glycation end product and advanced lipoxidation end product formation. J. Am. Soc. Nephrol. 11 (9), 1719–1725.
Nenna, A., Spadaccio, C., Lusini, M., Ulianich, L., Chello, M., Nappi, F., 2015. Basic and clinical research against advanced glycation end products (AGEs): new compounds to tackle cardiovascular disease and diabetic complications. Recent Pat. Cardiovasc. Drug Discov. 10 (1), 10–33.
Pradère, J.P., Hernandez, C., Koppe, C., Friedman, R.A., Luedde, T., Schwabe, R.F., 2016. Negative regulation of NF-κB p65 activity by serine 536 phosphorylation. Sci. Signal. 9 (442), ra85.
Rabbani, N., Thornalley, P.J., 2014. The critical role of methylglyoxal and glyoxalase 1 in diabetic nephropathy. Diabetes 63 (1), 50–52.
Rabbani, N., Xue, M., Thornalley, P.J., 2016. Dicarbonyls and glyoxalase in disease mechanisms and clinical therapeutics. Glycoconj. J. 33 (4), 513–525.
Sadowska-Bartosz, I., Galiniak, S., Bartosz, G., 2014. Kinetics of glycoxidation of bovine serum albumin by methylglyoxal and glyoxal and its prevention by various compounds. Molecules 19 (4), 4880–4896.
Sampath, C., Sang, S., Ahmedna, M., 2016. In vitro and in vivo inhibition of aldose reductase and advanced glycation end products by phloretin, epigallocatechin 3-gallate and [6]-gingerol. Biomed. Pharmacother. 84, 502–513.
Shao, X., Bai, N., He, K., Ho, C.T., Yang, C.S., Sang, S., 2008. Apple polyphenols, phloretin and phloridzin: new trapping agents of reactive dicarbonyl species. Chem. Res. Toxicol. 21 (10), 2042–2050.
Shao, X., Chen, H., Zhu, Y., Sedighi, R., Ho, C.T., Sang, S., 2014. Essential structural requirements and additive effects for flavonoids to scavenge methylglyoxal. J. Agric. Food Chem. 62 (14), 3202–3210.
Sompong, W., Adisakwattana, S., 2015. Inhibitory effect of herbal medicines and their trapping abilities against methylglyoxal-derived advanced glycation end-products. BMC Complement Altern. Med. 15 (1), 394.
Song, N., Ding, Y., Zhuo, W., He, T., Fu, Z., Chen, Y., Song, X., Fu, Y., Luo, Y., 2012. The nuclear translocation of endostatin is mediated by its receptor nucleolin in endothelial cells. Angiogenesis 15 (4), 697–711.
Tanikawa, T., Okada, Y., Tanikawa, R., Tanaka, Y., 2009. Advanced glycation end products induce calcification of vascular smooth muscle cells through RAGE/p38 MAPK. J. Vasc. Res. 46 (6), 572–580.
Verma, N., Manna, S.K., 2016. Advanced glycation end products (AGE) potently induce autophagy through activation of RAF protein kinase and nuclear factor κB (NF-κB). J. Biol. Chem. 291 (3), 1481–1491.
Wang, X., Chang, T., Jiang, B., Desai, K., Wu, L., 2007. Attenuation of hypertension development by aminoguanidine in spontaneously hypertensive rats: role of methylglyoxal. Am. J. Hypertens. 20 (6), 629–636.
Yamabe, S., Hirose, J., Uehara, Y., Okada, T., Okamoto, N., Oka, K., Taniwaki, T., Mizuta, H., 2013. Intracellular accumulation of advanced glycation end products induces apoptosis via endoplasmic reticulum stress in chondrocytes. FEBS J. 280 (7), 1617–1629.
Yu, W., Hu, X., Wang, M., 2018. Pterostilbene inhibited advanced glycation end products (AGEs)-induced oxidative stress and inflammation by regulation of RAGE/MAPK/NF-κB in RAW264. 7 cells. J. Funct. Foods 40, 272–279.
Zhang, H.B., Zhang, Y., Chen, C., Li, Y.Q., Ma, C., Wang, Z.J., 2016. Pioglitazone inhibits advanced glycation end product-induced matrix metalloproteinases and apoptosis by suppressing the activation of MAPK and NF-κB. Apoptosis 21 (10), 1082–1093.